Sleep Apnea Monitoring System Based on Channel State Information

Xiaolong Yang(✉), Xin Yu, Liangbo Xie, Mu Zhou, and Qing Jiang

School of Communication and Information Engineering, Chongqing University of Posts and Telecommunications, Chongqing, China
yangxiaolong@cqupt.edu.cn

Abstract. Sleep apnea is an important factor that affects human health. Traditional approaches based on wearable devices or pressure sensor devices are too expensive to be suitable for daily use, which also don't consider the impact on the breathing frequency when the human body turns over or gets up. In this paper, we propose a system based on WiFi to monitor sleep apnea state. Firstly, we use linear fitting to eliminate the phase errors of the receiving antennas, and wavelet transform to remove the noise of signal amplitude. Secondly, we combine the short-time Fourier transform and sliding window method to segment the signal. Finally, the features such as the variance of the phase difference between antennas are extracted, and the neural network model is built to identify apnea state, so as to eliminate interference caused by changes in sleep postures. Experiment results show that the detection accuracy rate for sleep apnea is over 95.6%. Our system can be a daily apnea monitoring approach and provide health reference for users.

Keywords: WiFi · Channel state information · Sleep apnea

1 Introduction

Sleep quality is closely related to human health. Some commercial devices collect data from headphones or wristbands worn by users to analyze the quality of sleep [1–3].

In recent years, because of its non-contact and high privacy characteristics, radar has been widely used in breathing detection. WiKiSpiro [4] monitors breathing in real time by combining a depth camera and a radar system. WiSpiro [5] is a system that uses frequency modulated continuous wave (FMCW) to re-construct the thorax and abdomen movement, and maps it to the breathing process through the training process. The Vital-Radio system [6] for monitoring breath and heart rate proposed by Adib et al. uses a bandwidth of 5.46 GHz to 7.25 GHz. However, radar system equipment is not only expensive to manufacture but also requires additional customized hardware equipment and has a high operating frequency.

Compared with radar systems, radio frequency identification (RFID) has the characteristics of simple structure and equipment, and high recognition rate. Therefore, it is also used for vital signs monitoring. Tagbreathe [7] attaches a lightweight RFID tag to

X. Wu et al. (Eds.): QShine 2020, LNICST 381, pp. 38–47, 2021.
https://doi.org/10.1007/978-3-030-77569-8_3

the user's clothing, analyzes the low-level data obtained by the RFID reader, and uses phase information to estimate the respiratory rate. With the popularity of WiFi devices, WiFi-based respiratory detection technology is gradually becoming a research hotspot. Ubibreathe [8] uses the received signal strength indication (RSSI) on the WiFi device for breath estimation. A bandpass filter with a cut-off frequency of 0.1 Hz to 0.5 Hz is used to filter the received RSSI signal. The Fourier transform is used to estimate the breathing frequency. However, it only provides accurate results when the human brings the WiFi device close to the chest.

Compared with the superimposed energy information provided by RSSI, channel state information (CSI) not only contains carrier amplitude information, but also provides phase information of each carrier. The finer granularity provides higher possibility for more accurate breath detection research. Liu [9] uses the CSI amplitude and phase difference to capture the tiny movements caused by breathing and heartbeat. Phasebeat [10] uses wavelet transform to decompose and reconstruct the respiratory signal and heart rate signal in the CSI signal. TR-BREATH [11] combines Root-Music and other algorithms to analyze the time-reversed resonance intensity to estimate the respiratory frequency.

In view of the above-mentioned shortcomings, the detection system for sleep proposed in this paper has strong privacy and low price, and is suitable for daily detection systems. Firstly, we construct the signal model of the received signal and modify the received CSI phase information. Secondly, we eliminate the noise, interference and abnormal values in the signal after the correction. Next, a signal segmentation algorithm is designed to select subcarriers that have the most obvious change in motion and segment the signal. Finally, we extract features from the segments and construct a classifier for detection and recognition. The scheme designed in this paper does not require any equipment to be carried, nor does it need to modify the related hardware equipment to detect the sleep state.

2 System Model and Framework

2.1 System Overview

In order to simulate the breathing state that may occur during sleep, the human is required to breathe normally in the test area to simulate the breathing state; stop breathing to simulate apnea; leave the test area to simulate unmanned state.

As shown in Fig. 1, the sleep state detection process based on WiFi is mainly divided into two stages. In the offline stage, CSI of unmanned state, human breathing state and apnea state are collected respectively. Then, we eliminate phase errors and noise interference in the environment, and select the optimal subcarrier. Finally, the features of the three scenes are extracted, and a detection classifier is constructed and generated. In the online phase, we collect CSI, preprocess signals, and extract signal features in the same way. The classifier built in the offline phase is used to complete the sleep state detection.

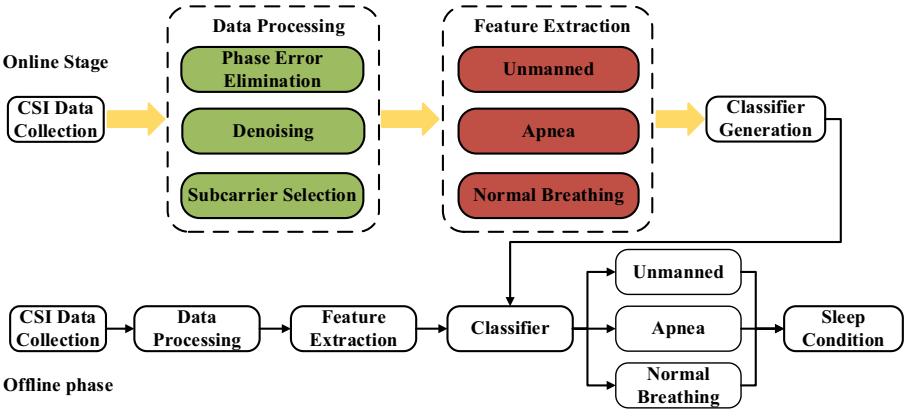

Fig. 1. A system architecture of a sleep apnea monitoring method based on home WiFi.

2.2 Channel State Information Overview

The advent of orthogonal frequency division multiplexing (OFDM) technology helps us extract CSI from the transmitting end to the receiving end of the wireless signal. To characterize multipath propagation, wireless channels are usually modeled with channel impulse response (CIR). It can be expressed as:

$$h(t) = \sum_{l=1}^{L} \alpha_l \delta(t - \tau_l) \tag{1}$$

where L is the total number of propagation paths; $\delta(t)$ is the Dirichlet function; α_l and τ_l are the amplitude attenuation and time delay of the i-th path, respectively. Since multipath transmission shows frequency selective fading in the frequency domain, it can also be characterized by channel frequency response (CFR) $H(f)$. CFR and CIR are Fourier transforms:

$$H(f) = \mathrm{FT}[h(t)] = \sum_{l=1}^{L} \alpha_l e^{-j2\pi f \tau_l} \tag{2}$$

where f is the frequency. In the time domain, the accepted signal $y(t)$ is the convolution of the transmitted signal $s(t)$ and $h(t)$:

$$y(t) = s(t) \otimes h(t) \tag{3}$$

Correspondingly, in the frequency domain, the received signal spectrum $Y(f)$ is the product of the transmitted signal spectrum $S(f)$ and $H(f)$:

$$Y(f) = S(f) \cdot H(f) \tag{4}$$

CSI is the sampled version of CFR. Assuming that there are K subcarriers on one antenna and M packets are received, the CSI can be expressed as a matrix:

$$\mathbf{CSI}_{K\times M} = \begin{bmatrix} csi_{1,1} & csi_{1,2} & \cdots & csi_{1,M} \\ \vdots & \vdots & \ddots & \vdots \\ csi_{K,1} & csi_{K,2} & \cdots & csi_{K,M} \end{bmatrix} \tag{5}$$

where $csi_{k,m}(k \in [1, K],\ m \in [1, M])$ represents the sum of all paths of the k-th subcarrier in the m-th data packet.

3 Data Processing

3.1 Phase Error Elimination

In actual operation, the actual received phase consists of the true phase value and the offset value:

$$\hat{\phi}_k = \phi_k + \frac{2\pi}{K} k\eta + \rho \tag{6}$$

where $\hat{\phi}_k$ and ϕ_k represent measured phase and actual phase of the k-th subcarrier, respectively. η represents the phase offset and ρ represents constant error. In this paper, the phase error is eliminated by linear fitting method [12], and the result comparison is shown in Fig. 2. It can be seen that the phase after linear calibration is more stable than the original phase. Although the processed phase is not completely equal to the true phase, it is very close to the true value, and the error can be relatively ignored.

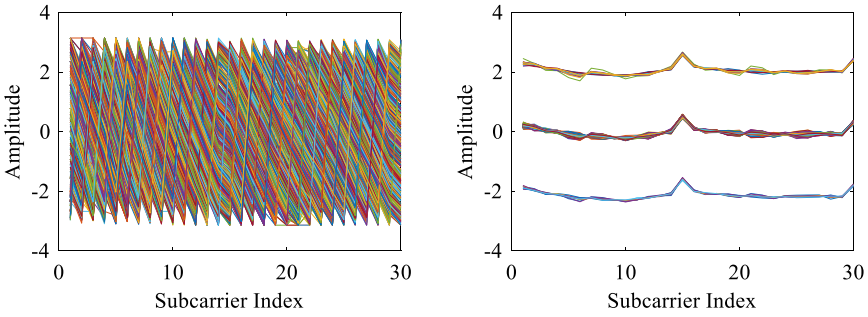

(a) Subcarrier phase before linear error cancellation.

(b) Subcarrier phase after linear error cancellation.

Fig. 2. The comparison result before and after the subcarrier phase linearity error is eliminated.

3.2 Noise Cancellation

In the measured environment, due to the multipath effect in the room and the factors of the device, the received signal exists various noises, resulting in the required useful signals being submerged in the noise. Thus, the process of amplitude processing of CSI in this paper includes the removal of outliers and wavelet denoising. As shown in the black box in Fig. 3(a), there will always be a few outliers that deviate from the original signal trajectory. We use a filter based on the median absolute deviation to filter out the sample values outside of $[\mu - 3 \cdot \sigma, \mu + 3 \cdot \sigma]$, where μ represents the mean, and σ represents the standard deviation. Then, we replace them by the median of the data, as shown in Fig. 3(b).

After removing the influence caused by outliers, the wavelet denoising method is used to process the CSI amplitude. In this paper, 'db3' is used as a wavelet basis to decompose the signal in 5 layers. The comparison results before and after denoising are shown in Fig. 4. Before denoising, the signal is submerged in noise, and after denoising, the waveform becomes smooth and can reflect the changing state of the channel.

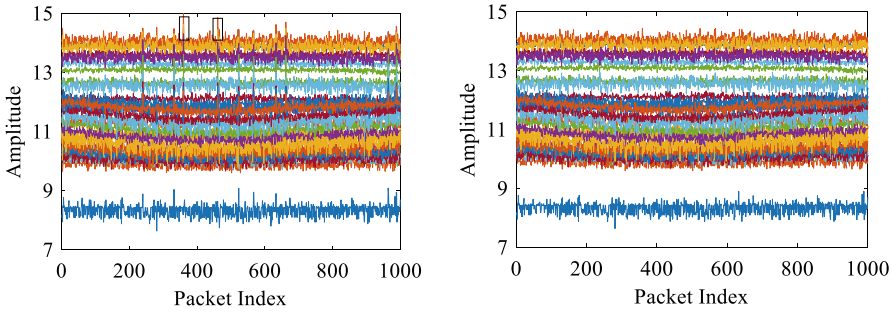

(a) CSI amplitude before removing outliers. (b) CSI amplitude after removing outliers.

Fig. 3. CSI amplitude before and after removing outliers.

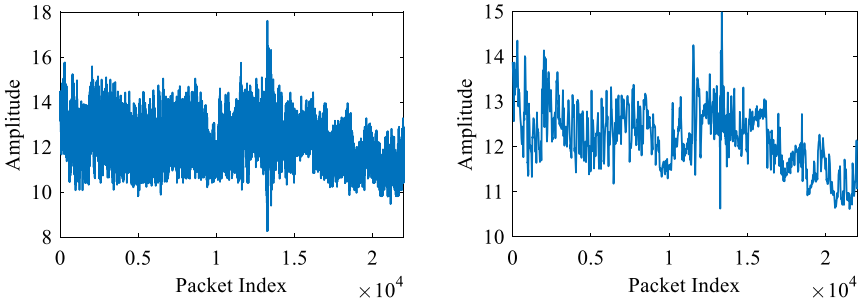

(a) CSI amplitude before removing high frequency noise. (b) CSI amplitude after removing high frequency noise.

Fig. 4. Comparison of CSI amplitude before and after denoising.

3.3 Subcarrier Selection Method

Due to the different frequency of the subcarriers, the sensitivity to changes caused by human breathing, apnea and unmanned states is also different. Therefore, we need to filter out subcarriers that do not change significantly. In this paper, we use the change of CSI amplitude to quantify the sensitivity of subcarriers to the sleep state. Assuming that the signal length is M, we calculate the variance of the CSI signal of the k-th subcarrier V_k:

$$V_k = \frac{1}{M-1}\sum_{m=1}^{M}(csi_{k,m} - \frac{1}{M}\sum_{m=1}^{M} csi_{k,m})^2 \tag{7}$$

4 Feature Extraction

4.1 Signal Segmentation Method

Since the collected data may contain the subject being in apnea or the subject leaving the test area, etc., for monitoring the sleep state accurately, before performing feature extraction, these fragments need to be segmented from the data, and identify and classify them. Therefore, this paper uses a sliding window-based method [13] to segment the signal. We assume that the window length is N and the signal length is M, and calculate the variance V_n of the CSI signal difference between two adjacent windows:

$$\begin{aligned} V_n = \frac{1}{N-1}\sum_{m=1}^{N}((csi_{n,m} - csi_{n-1,m}) \\ - \frac{1}{N}\sum_{m=1}^{N}(csi_{n,m} - csi_{n-1,m}))^2 \end{aligned} \tag{8}$$

where n indicates the number index of windows. Then, We normalize V_n to get V_n':

$$V_i' = \frac{V_i - \min\{V_i\}}{\max\{V_i\} - \min\{V_i\}}, \quad (1 \le i \le n) \tag{9}$$

Firstly, we set the start flag as "False". When it is "False", compare each V_i' with the threshold σ. If $V_i^{'} \ge \lambda$, we set the start time $T_{begin} = (i-1)\cdot N$ and change the start flag to "True". When the start flag is "True", if $V_i^{'} < \lambda$, we set the middle Node $V_{test}^{'}$ as $\omega \cdot V_i^{'} + (1-\omega)\cdot V_{i+1}^{'}$. To make a judgment to $V_{test}^{'}$, if $V_{test}^{'} < \beta \cdot V_{i+1}^{'}$, we set the end time node $T_{end} = i \cdot N$. After traversing all V_n', we can get the start and end time node of all the fragments. In this paper, we set the threshold λ as 0.65, and the weighted parameters ω and β as 0.85 and 3, respectively.

4.2 Feature Extraction

In this paper, we use the difference in phase difference between antennas in the presence of human breathing, apnea, and absence to detect the sleep state of the human. We calculate the phase difference D between the antennas, and the mean, variance, range and quartile moment of it:

$$\begin{cases} E_D = \frac{1}{M}\sum_{m=1}^{M} D(m) \\ V_D = \frac{1}{M-1}\sum_{m=1}^{M} (D(m) - E_D)^2 \\ R_D = \max(D) - \min(D),\ D' = sort(D), \\ Q_D = D'((M+1)\cdot 0.75) - D'((M+1)\cdot 0.25) \end{cases} \tag{10}$$

where $sort(\cdot)$ means sort from small to large. Assuming that the number of antennas, subcarriers and collected samples are X, K and Y, respectively, the input feature dimension of the classifier is $2X \cdot (X-1) \cdot K \times Y$. In this paper, back-propagation (BP) neural network is used to learn and map the feature set.

5 Experimental Results

In this paper, we utilize the csitools based on Linux and use the form of one transmitter and three receivers. The transmitting end uses a directional antenna to send data, and the receiving end uses three omnidirectional antennas to receive data. We use two mini hosts equipped with Intel 5300 wireless network card as transmitter and receiver and select channel 149 with a center frequency of 5.749 GHz to send and receive data. The packet sending rate is set to 500 per second. The offline data collected in the experiment are in three states: unmanned, apnea, and human breathing. 450 sets of data were collected respectively to extract features to form the training data set.

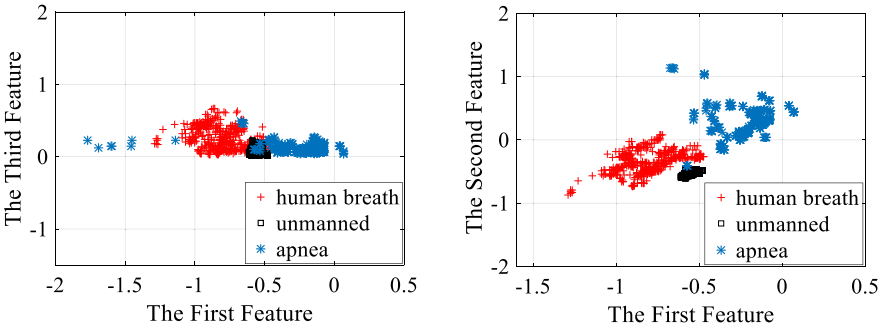

(a) Scatterplot of the distribution of the first and third features.

(c) Scatterplot of the distribution of the first and second features.

Fig. 5. Scatterplot of feature distribution.

For feature extraction, we observe the performance of the extracted signal feature through the feature distribution map, and randomly take two of the features to draw a feature distribution scatter plot, as shown in Fig. 5. As can be seen from Fig. 5(a), there is a small amount of confusion between the first feature and the third feature due to the similarity between apnea and unmanned state. But from Fig. 5(b), the first feature and the second feature are almost free of mixed grains and has a clear distribution area, which can better distinguish the three states.

The confusion matrix obtained after the classification is shown in Fig. 6. Then, we calculate its Precision and precision Recall:

$$\begin{cases} \text{Precision} = \dfrac{TP}{TP + FP} \\ \text{Recall} = \dfrac{TP}{TP + FN} \end{cases} \tag{11}$$

	human breath	apnea	unmanned
human breath	99.1%	0.7%	0.2%
apnea	4.0%	95.6%	0.4%
unmanned	0.0%	0.4%	99.6%

Fig. 6. Classification confusion matrix of three states.

Combining Fig. 6 and (11), the Precision and Recall values for presence of breath, apnea, and unmanned states are 96.12%, 98.85%, 99.33%, 99.11%, 95.56%, 99.56%, respectively. Then, we use macro F1-Score as a measurement indicator to weight it on average:

$$macro\,F_1\text{-}score = 2\times \frac{\frac{1}{3}\cdot\sum_{j=1}^{3}\text{Precision}(j)\times\frac{1}{3}\cdot\sum_{j=1}^{3}\text{Recall}(j)}{\frac{1}{3}\cdot\sum_{j=1}^{3}\text{Precision}(j)+\frac{1}{3}\cdot\sum_{j=1}^{3}\text{Recall}(j)} \tag{12}$$

The calculated Macro F1-Score is about 0.98. For the accuracy and recall rate in the macro F1-Score comprehensive model, the greater the value is, the higher the quality of the classification model is. Compared with the common CSI-based breathing detection system, this article fully considers the effect caused by getting up and turning over during actual sleep, and abstracts effective data segment without interferences produced by human's movement. The detection accuracy rate can reach more than 95.6%. Compared with the existing breath detection scheme, the scheme proposed in this paper has more practical application value.

6 Conclusion

In this paper, we propose a WiFi-based sleep apnea state detection system that does not require the subject to wear any additional equipment or modify the hardware facilities, which can complete the sleep state only using commercial WiFi equipment. Firstly, we construct the signal model and preprocess the received signal. Then, we design a segmentation algorithm to select the optimal subcarrier and segments the signal. Finally, the features of segments are extracted, and a classifier is constructed to recognize breath, apnea and unmanned state in the sleep state. Experimental results show that this approach can not only eliminate the noise CSI information, but also achieve a recognition accuracy rate of more than 95.6%. How to recognize and detect sleep status for multiple people will become our future work.

Acknowledgment. This work was supported by the National Natural Science Foundation of China (61771083, 61704015), Science and Technology Research Project of Chongqing Education Commission (KJQN201800625), and Chongqing Natural Science Foundation Project (cstc2019jcyj-msxmX0635).

References

1. http://www.toodaylab.com/44685/
2. http://www.fitbit.com/
3. Shambroom, J.R., Fábregas, S.E., Johnstone, J.: Validation of an automated wireless system to monitor sleep in healthy adults. J. Sleep Res. **21**(2), 221–230 (2012)
4. Nguyen, P., Transue, S., Choi, M.H.: WiKiSpiro: non-contact respiration volume monitoring during sleep. In: The Eighth Wireless of the Students, by the Students, and for the Students Workshop. ACM, pp. 27–29 (2016)
5. Nguyen, P., Zhang, X., Halbower, A.: Continuous and fine-grained breathing volume monitoring from afar using wireless signals. In: IEEE INFOCOM 2016-IEEE Conference on Computer Communications, pp. 10–14. IEEE (2016)
6. Adib, F., Mao, H., Kabelac, Z.: Smart homes that monitor breathing and heart rate. In: Proceedings of the ACM Conference on Human Factors in Computing Systems. ACM, pp. 837–846 (2015)
7. Hou, Y., Wang, Y., Zheng, Y.: TagBreathe: monitor Breathing with Commodity RFID Systems. In: 2017 IEEE 37th International Conference on Distributed Computing Systems (ICDCS), pp. 969–981. IEEE (2017)
8. Abdelnasser, H., Harras, K.A., Youssef, M.: Ubibreathe: a ubiquitous noninvasive wifi-based breathing estimator. In: China Proceedings of the IEEE MobiHoc, no. 15, pp. 277–286 (2015)
9. Liu, J., Wang, Y., Chen, Y.: Tracking vital signs during sleep leveraging off-the-shelf wifi. In: ACM International Symposium. ACM, pp. 267–276 (2015)
10. Wang, X., Yang, C., Mao, S.: PhaseBeat: exploiting CSI phase data for vital sign monitoring with commodity WiFi devices. In: Proceedings of the 2017 IEEE International Conference on Distributed Computing Systems (ICDCS), pp. 1230–1239 (2017)
11. Chen, C., Han, Y., Chen, Y.: TR-BREATH: time-reversal breathing rate estimation and detection. IEEE Trans. Biomed. Eng. **65**(3), 489–501 (2017)

12. Li, F., Xu, C., Liu, Y.: Mo-sleep: Unobtrusive sleep and movement monitoring via WiFi signal. In: 2016 IEEE 35th International Performance Computing and Communications Conference, Las Vegas, pp. 173–180 (2016)
13. Wu, X., Chu, Z., Yang, P.: TW-See: human activity recognition through the wall with commodity wifi devices. IEEE Trans. Veh. Technol. **68**(1), 306–319 (2019)